

Lifshitz quantum phase transitions and Fermi surface transformation with hole doping in high- T_c superconductors

S.G. Ovchinnikov,^{1,2} M.M. Korshunov,^{1,3,4} and E.I. Shneyder^{1,5,*}

¹*L.V. Kirensky Institute of Physics, Siberian Branch of Russian Academy of Sciences, 660036 Krasnoyarsk, Russia*

²*Siberian Federal University, Krasnoyarsk, 660041, Russia*

³*Max-Planck-Institut für Physik komplexer Systeme, D-01187 Dresden, Germany*

⁴*Department of Physics, University of Florida, Gainesville, Florida 32611, USA*

⁵*Reshetnev Siberian State Aerospace University, Krasnoyarsk 660014, Russia*

(Dated: October 28, 2018)

We study the doping evolution of the electronic structure in the normal phase of high- T_c cuprates. Electronic structure and Fermi surface of cuprates with single CuO_2 layer in the unit cell like $\text{La}_{2-x}\text{Sr}_x\text{CuO}_4$ have been calculated by the LDA+GTB method in the regime of strong electron correlations (SEC) and compared to ARPES and quantum oscillations data. We have found two critical concentrations, x_{c1} and x_{c2} , where the Fermi surface topology changes. Following I.M. Lifshitz ideas of the quantum phase transitions (QPT) of the 2.5-order we discuss the concentration dependence of the low temperature thermodynamics. The behavior of the electronic specific heat $\delta(C/T) \sim (x - x_c)^{1/2}$ is similar to the Loram and Cooper experimental data in the vicinity of $x_{c1} \approx 0.15$.

PACS numbers: 71.27.+a; 74.72.-h; 75.40.-s

I. INTRODUCTION

Nowadays high- T_c cuprates is the second most studied class of condensed matter after semiconductors. Both the nature of the superconductivity and the abnormal pseudogap feature of the normal phase are not clear yet^{1,2,3,4,5,6,7,8}. A lot of experimental data on the electronic structure have been obtained by ARPES that reveals the doping evolution of the Fermi surface (FS) from small arcs near $(\pi/2, \pi/2)$ at small doping to the large FS around (π, π) at large doping⁹. Quantum oscillations measurements in strong magnetic fields on the single crystals $\text{YBa}_2\text{Cu}_3\text{O}_{6.5}$ ¹⁰ and $\text{YBa}_2\text{Cu}_4\text{O}_8$ ¹¹ have proved the existence of small hole pockets in the underdoped (UD) cuprates that looks as a contradiction to the ARPES arcs. This contradiction has been explained by the interaction between holes and spin fluctuations in the pseudogap state with the existing short-range antiferromagnetic (AFM) order^{12,13,14,15}. It occurs that the part of the hole pocket related to the shadow band has smaller quasiparticle (QP) lifetime due to the QP scattering on spin fluctuations. Recently VUV laser ARPES¹⁶ has found a closed FS pocket in the UD La-Bi2201 with the small intensity at the shadow band part. The strong interaction of the electrons with the spin fluctuations is a general property of SEC systems and takes place not only in cuprates but also *e.g.* in manganates¹⁷.

The conventional LDA (local density approximation) approach to the electronic structure in the regime of SEC fails. Various realistic multiband models of CuO_2 layer in cuprates in the low energy region result in the effective Hubbard and $t - J$ models^{18,19,20,21,22}. In the hybrid LDA+GTB scheme²³ that combines the LDA calculations of the multiband $p - d$ model parameters and the generalized tight-binding (GTB) treatment of SEC the low energy effective $t - t' - t'' - J^*$ model has been ob-

tained from microscopic approach with all parameters being calculated *ab initio*.

Small hole pockets in the UD case with area $\sim x$ appear in a theory considering the hole dynamics in the AFM spin background and have been obtained by the exact diagonalization²⁴ and the Quantum Monte Carlo studies of the finite clusters^{25,26} as well as by various variational and perturbation calculations for the infinite-dimension lattice^{27,28,29,30,31}. Once the long-range AFM order disappears with doping the electronic structure calculations in the paramagnetic phase results in the dispersion of the valence band with the top at (π, π) and the large FS³². Still there are apologists of the “universal metal dispersion” calculating the LDA band structure and the FS and claiming the rigid band behavior with Fermi level shift of the fixed band dispersion³³. After the small hole pockets were discovered in the Landau oscillations experiments^{10,11}, the rigid band scenario becomes evidently unconvincing. In place of conventional Fermi liquid state of the normal metal, the pseudogap state appears in the phase diagram of cuprates beside the long-range AFM phase. Though the origin of the pseudogap state is still debated, the contribution of the fluctuating short-range AFM order is clear⁵. The short-range AFM order is essential not only in the UD region. Even at the optimal doping the AFM correlation length $\xi_{AFM} \approx 10\text{\AA}$ ³⁴. At low temperatures $T \leq 10\text{K}$, spin fluctuations are slow with the typical time scale 10^{-9}sec . and on the spatial scale of ξ_{AFM} (size of the AFM microdomain)³⁵. This time is large in comparison to the fast electronic lifetime in ARPES ($\sim 10^{-13}\text{sec}$)³⁶ and to the cyclotron period $T \sim 2\pi\omega_c^{-1} \sim 10^{-12}$ with ω_c being a cyclotron frequency in quantum oscillations experiments^{10,11}. Thus we safely consider that the spin fluctuations are frozen at low T and take into account only the spatial dependence of the short-range AFM or-

der. It means that the electronic self-energy $\Sigma(k, \omega)$ will depend only on momentum, $\Sigma(k, \omega) \rightarrow \Sigma(k)$.

We use this approach to study the concentration dependence of the electronic structure and the FS. In Section 2 we present the electronic structure and the change of the FS topology within $t - t' - t'' - J^*$ model. The FS area and the Luttinger theorem are also discussed. In Section 3 we give the qualitative picture based on the interaction between hole and spin fluctuations. In Section 4 we use the Lifshitz ideas^{37,38} on the QPT to study the low temperature thermodynamics. The electronic specific heat singularity near QPT is compared to the experimental data³⁹.

II. THE FERMI SURFACE OF $La_{2-x}Sr_xCuO_4$ AND ITS DOPING EVOLUTION

Within the LDA+GTB approach we start from the *ab initio* LDA calculations and construct the Wannier functions in the basis of oxygen p -orbitals and copper e_g -orbitals. The multiband $p - d$ model⁴⁰ parameters are calculated *ab initio*. Then we apply the cluster perturbation approach^{18,41} and introduce the Hubbard X -operators constructed within the full set of eigenstates of the unit cell (the CuO_6 cluster) that is obtained by exact diagonalization of the multiband $p - d$ model Hamiltonian of the cluster. By the GTB method we construct the low energy effective Hubbard model with $U = E_{CT}$, where E_{CT} is the charge transfer gap⁴². In the Hubbard model, the $X_f^{0\sigma}$ operator describes the hole annihilation at the site f in the lower Hubbard band (LHB) of holes that corresponds to the electron at the bottom of the conduction band. The hole annihilation in the upper Hubbard band (UHB) is given by the $X_f^{\bar{\sigma}2}$ operator and corresponds to the electron at the top of the valence band. In the limit of SEC, $U_{eff} \gg t$ (t is the effective intersite hopping), we may exclude either two-hole state $|2\rangle$ and obtain the effective Hamiltonian for LHB or two-electron state $|0\rangle$ (hole vacuum $d^{10}p^6$) and to get the effective Hamiltonian for UHB. Latter case is interesting for the hole doped cuprates. We emphasize that the effective $t - t' - t'' - J^*$ model is derived from the microscopic approach and its parameters are calculated *ab initio*. Here J^* means that we take into account the 3-site correlated hopping that is of the same order as the superexchange interaction J .

The model Hamiltonian is given by

$$\begin{aligned} H_{t-J^*} &= H_{t-J} + H_{(3)}, \\ H_{t-J} &= \sum_{f,\sigma} [(\varepsilon - \mu)X_f^{\sigma\sigma} + (\varepsilon_2 - 2\mu)X_f^{22}] \\ &+ \sum_{f \neq g, \sigma} t_{fg}^{11} X_f^{2\bar{\sigma}} X_g^{\bar{\sigma}2} + \sum_{f \neq g} J_{fg} \left(\vec{S}_f \cdot \vec{S}_g - \frac{1}{4} n_f n_g \right) \\ H_{(3)} &= \sum_{f \neq m \neq g, \sigma} \frac{t_{fm}^{01} t_{mg}^{01}}{U_{eff}} (X_f^{\sigma 2} X_m^{\bar{\sigma}\sigma} X_g^{2\bar{\sigma}} - X_f^{\bar{\sigma}2} X_m^{\sigma\sigma} X_g^{2\bar{\sigma}}). \end{aligned} \quad (1)$$

Here $J_{fg} = 2 \left(t_{fg}^{01} \right)^2 / U_{eff}$, t_{fg}^{01} is the interband (LHB \leftrightarrow UHB) hopping parameter between two sites f and g , \vec{S}_f is the spin operator, ε and ε_2 are one- and two-hole local energies, and μ is the chemical potential. The intraband hopping parameters t_{fg}^{11} have been calculated up to 6-th nearest neighbors. It appears that only 3 coordination spheres are important and contribution to the hole dispersion of the more distant neighbors is negligible. The calculated from *ab initio* model parameters for $La_{2-x}Sr_xCuO_4$ are (in eV):

$$\begin{aligned} t &= 0.932, \quad t' = -0.12, \quad t'' = 0.152, \\ J &= 0.298, \quad J' = 0.003, \quad J'' = 0.007. \end{aligned} \quad (2)$$

We introduce the hole Green function in the UHB (here $\bar{\sigma} \equiv -\sigma$)

$$G_\sigma(\mathbf{k}, E) = \langle\langle X_{\mathbf{k}}^{\bar{\sigma}2} | X_{\mathbf{k}}^{2\bar{\sigma}} \rangle\rangle_E. \quad (3)$$

The analysis of the whole set of diagrams in the X -operators diagram technique results in the following exact generalized Dyson equation⁴³

$$G_\sigma(\mathbf{k}, E) = \frac{P_\sigma(\mathbf{k}, E)}{E - \varepsilon_0 + \mu - P_\sigma(\mathbf{k}, E)t_{\mathbf{k}} - \Sigma_\sigma(\mathbf{k}, E)}. \quad (4)$$

Here $t_{\mathbf{k}}$ is the Fourier transform of the hopping, $P_\sigma(\mathbf{k}, E)$ and $\Sigma_\sigma(\mathbf{k}, E)$ are the strength and the self-energy operators. In the simplest Hubbard I approximation $\Sigma_\sigma = 0$, $P_\sigma = F_{\bar{\sigma}2} = \langle X_f^{\bar{\sigma}\bar{\sigma}} \rangle + \langle X_f^{22} \rangle$. The QP spectral weight is determined by the filling factor $F_{\bar{\sigma}2}$. In the diagram technique, $F_{\bar{\sigma}2}$ corresponds to the so-called ‘‘terminal factors’’⁴⁴.

To incorporate the effect of the short-range AFM order on the QP dynamics we go beyond the Hubbard I approximation. The calculation scheme is given in Ref. 45. We use the Mori-type method to project the higher order Green functions to the single particle function (3). A similar approach that took spin dynamics into the account was used in Refs. 22,46. The hole concentration in $La_{2-x}Sr_xCuO_4$ (LSCO) per unit cell is $n_h = 1 + x$. The completeness condition for the local Hilbert space in the $t - J$ model is

$$\sum_{\sigma} X_f^{\sigma\sigma} + X_f^{22} = 1. \quad (5)$$

Thus we easily obtain $\langle X_f^{\sigma\sigma} \rangle = (1 - x)/2$, $\langle X_f^{22} \rangle = x$, and $F_{\bar{\sigma}2} = (1 + x)/2$. The Green function (3) becomes

$$G_\sigma(\mathbf{k}, E) = \frac{(1 + x)/2}{E - \varepsilon_0 + \mu - \frac{1+x}{2} t_{\mathbf{k}} - \frac{1-x^2}{4} \frac{(t_{\mathbf{k}}^{01})^2}{U_{eff}} - \Sigma(\mathbf{k})}, \quad (6)$$

with the self energy given by

$$\Sigma(\mathbf{k}) = \frac{2}{1+x} \frac{1}{N} \sum_{\mathbf{q}} \left\{ \left[t_{\mathbf{q}} - \frac{1-x}{2} J_{\mathbf{k}-\mathbf{q}} - x (t_{\mathbf{q}}^{01})^2 / U_{eff} - (1+x) t_{\mathbf{k}}^{01} t_{\mathbf{q}}^{01} / U_{eff} \right] K(\mathbf{q}) \right. \quad (7)$$

$$\left. + \left[t_{\mathbf{k}-\mathbf{q}} - \frac{1-x}{2} \left(J_{\mathbf{q}} - (t_{\mathbf{k}-\mathbf{q}}^{01})^2 / U_{eff} \right) - (1+x) t_{\mathbf{k}}^{01} t_{\mathbf{k}-\mathbf{q}}^{01} / U_{eff} \right] \cdot \frac{3}{2} C(\mathbf{q}) \right\}. \quad (8)$$

Here $K(\mathbf{q})$ and $C(\mathbf{q})$ stand for the Fourier transforms of the static kinetic and spin correlation functions,

$$\begin{aligned} K(\mathbf{q}) &= \sum_{\mathbf{f}-\mathbf{g}} e^{-i(\mathbf{f}-\mathbf{g})\mathbf{q}} \langle X_{\mathbf{f}}^{2\bar{\sigma}} X_{\mathbf{g}}^{\bar{\sigma}2} \rangle, \\ C(\mathbf{q}) &= \sum_{\mathbf{f}-\mathbf{g}} e^{-i(\mathbf{f}-\mathbf{g})\mathbf{q}} \langle X_{\mathbf{f}}^{\sigma\bar{\sigma}} X_{\mathbf{g}}^{\bar{\sigma}\sigma} \rangle \\ &= 2 \sum_{\mathbf{f}-\mathbf{g}} e^{-i(\mathbf{f}-\mathbf{g})\mathbf{q}} \langle S_{\mathbf{f}}^z S_{\mathbf{g}}^z \rangle. \end{aligned} \quad (9)$$

For the LHB which corresponds to the electron-doped cuprates, the similar Green function has been obtained previously⁴⁷. We assume that the spin system is an isotropic spin liquid with any averaged component of the spin being zero and the equal correlation functions for any component of the spin, $\langle S_f^\alpha S_g^\alpha \rangle$, $\alpha = x, y, z$. We calculate this correlation function following Ref. 47 by the method developed previously for the Heisenberg model^{48,49}. The resulting static magnetic susceptibility agrees with the other calculations for the $t-J$ model^{50,51}. As concerns the kinetic correlation function it is expressed via the same Green function (3).

The self-consistent treatment of the electronic and spin systems results in the evolution of the correlation functions (9), the chemical potential, and the FS as function of doping (Fig. 1). At a small doping we get 4 hole pockets close to $(\pi/2, \pi/2)$ point as was expected for the AFM state. At the critical concentration $x_{c1} \approx 0.15$ the connection of this pockets appears along the $(\pi, 0) - (\pi, \pi)$ line and the FS topology changes. At $x_{c1} < x < x_{c2} \approx 0.24$ we obtain two FS centered around the (π, π) point. The smaller one is the electronic FS; it shrinks with doping and collapsed when $x \rightarrow x_{c2}$. The larger one is the hole FS; with increasing x it becomes more rounded. At $x > x_{c2}$ only a large hole FS remains. Finally there is one more change of the topology at $x = x_{c3}$ when the FS touches the $(\pi, 0)$ point and becomes of electronic type centered around the $(0, 0)$ point.

Note that the values of critical concentrations are obtained with the finite accuracy. First of all, model parameters are deduced by the complicated procedure involving the projection of the LDA wave functions in Wannier function basis and may vary with the change of this basis. Second, the equation for the Green function (6) is approximate and taking into account higher order corrections may change values of the critical concentrations quantitatively. On the other hand, the qualitative picture should remain unchanged since it is due to the general

properties of the electron scattering by the AFM fluctuations. Also, the qualitatively similar transformation of the FS with doping has been obtained for the Hubbard model in the regime of SEC (Fig. 15 in Ref. 46), in the spin-density wave state of the Hubbard model⁶⁴, for the spin-fermion model⁶⁵, and in the *ab initio* multielectron quantum chemical approach⁶⁶. Qualitative agreement of our results and results of calculations in different approximations^{46,64,65,66} is basically due to the common underlying idea: the change of the electron dispersion caused by the interaction with the short-range AFM order. However, in our approach both magnetic and electronic properties are treated self-consistently.

In Fig. 1 we also show the ARPES data on $\text{Bi}_2\text{Sr}_{2-x}\text{La}_x\text{CuO}_{6+y}$ (Bi2201) from Ref. 52 and the recent data¹⁶ on LSCO for doping concentrations 0.10, 0.12, and 0.16. The single crystals of Bi2201 have been studied experimentally with different hole concentrations, $0.05 < p < 0.18$. This crystal has one CuO_2 layer in the unit cell - that is why our calculations appropriate for LSCO can be used for Bi2201 with the condition $x = p$. The question arise whether the model parameters are the same or different for the two crystals? In the conventional single electron tight-binding model used in Ref. 52 to fit the ARPES data the hopping parameters depend on doping significantly. That is why the authors of Ref. 52 claim that the ratio t'/t is different for Bi2201 and LSCO. However, as evident from figures 5a and 5b of Ref. 52, for the lowest doping the hopping values are close to each other for both substances. The reason is that hopping parameters depend on the interatomic distance that is almost the same in Bi2201 and LSCO. That is why we use the same parameters for all doping concentrations. The doping dependence of the band structure and its non-rigid behavior comes up as the effect of SEC. One of the main players in this game is the filling factor $F_{\bar{\sigma}2}$.

Comparing our calculated FS with the experimental data in Fig. 1 we notice that for $x = 0.05, 0.07, 0.10$, and 0.12 the experimental Fermi arc position is close to the calculated inner part of the hole pocket (the part which is near the $(0, 0)$ point). The outer part appears as the small intensity signal at $x = 0.10$ and $x = 0.12$ in ARPES. After the Lifshitz QPT at $x_{c1} = 0.15$ we see the two parts of the FS in agreement with ARPES data⁵². Usually the outer FS (the nearest to (π, π) point) in Bi-cuprates is ascribed as the superlattice reflection. It may be that the superlattice signal simply mask the part of the FS that we obtain in the calculation. An-

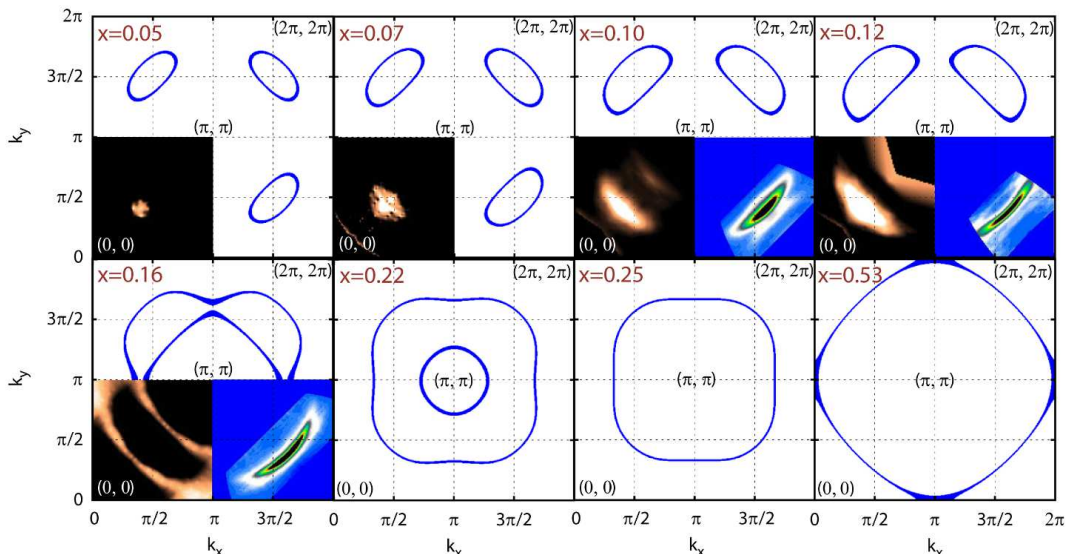


FIG. 1: Calculated Fermi surface for a single-layer cuprate for different doping levels x . Fermi surface topology changes at $x_{c1} = 0.15$ and $x_{c2} = 0.24$. ARPES data from Ref. 52 and Ref. 16 are shown in lower left and lower right corners of the Brillouin zone, respectively.

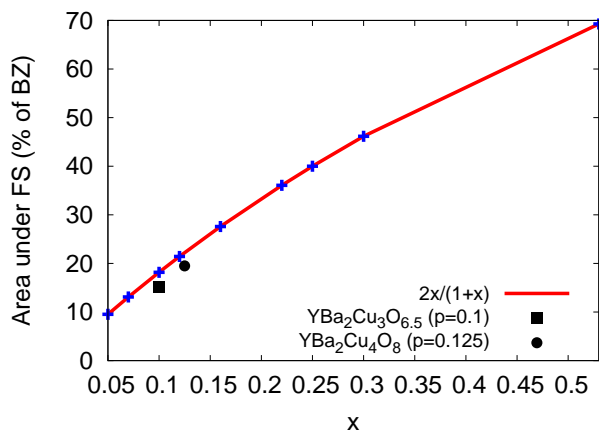


FIG. 2: The doping dependence of the FS area (in % of the Brillouin zone area) calculated directly (+), from the generalized Luttinger theorem (solid line). The experimental values from the quantum oscillations data^{10,11} are also shown.

other most probable explanation is that the scattering by the AFM fluctuations suppresses intensity of the spectral peaks corresponding to the outer FS. We will discuss this scenario in the next Section.

At higher doping the ARPES results in the large hole pocket centered around the (π, π) point⁵³, *e.g.* in $\text{Tl}_2\text{Ba}_2\text{CuO}_{6+y}$ with $p = 0.26$. Our calculations result in such topology for $x > x_{c2}$. According to Ref. 68, there is an electron pocket for LSCO at $x = 0.30$.

Now we would like to discuss the FS area and the Luttinger theorem. In Fig. 2 we give the FS area as a function of doping. Note that the standard formulation of the Luttinger theorem does not work for Hubbard fermions.

For free electrons each quantum state in the k -space contains 2 electrons with opposite spins. The spectral weight of the Hubbard fermion is determined by the strength operator, $P_\sigma = F_{\bar{\sigma}2}$, and each quantum state contains $2F_{\bar{\sigma}2} = 1 + x$ electrons. A generalized Luttinger theorem for SEC system⁶⁷ takes into account the spectral weight of each $|k\rangle$ state. For LSCO the hole concentration $n_h = 1 + x$, so the electron concentration $n_e = 1 - x$. Using the dispersion law (see Fig. 3b below) we calculate the number of occupied electronic states N_k^e below the Fermi level. The electronic concentration $n_e = 2F_{\bar{\sigma}2}N_k^e = 1 - x$. It gives us $N_k^e = (1 - x)/(1 + x)$. Then the number of free (occupied by holes) k -states is $N_k^h = 1 - N_k^e = 2x/(1 + x)$, and the FS area in Fig. 2 is determined by this number. The FS area obtained by direct calculation of the occupied k -state under the Fermi level is shown by crosses. Two available FS areas from the quantum oscillations data^{10,11} are also marked in the Fig. 2. It is evident and very important that the Luttinger theorem is not applicable in the standard formulation. On the other hand, its generalization for the case of correlated Hubbard fermions describes the experimental data very well.

III. QUALITATIVE ANALYSIS OF THE ELECTRON DISPERSION AND ARPES IN A SYSTEM WITH THE SHORT-RANGE AFM BACKGROUND

It was shown earlier^{12,13,14,15} that AFM fluctuations transform the closed hole pocket into the arc. We will extend the same arguments to the doping region where AFM fluctuations are strong. The electron Green function on the square lattice with electron scattering by the

Gaussian fluctuations that imitate the short-range AFM order with $Q = (\pi, \pi)$ is equal to¹⁵

$$G_D(\mathbf{k}, E) = \frac{E - \varepsilon(\mathbf{k} + \mathbf{Q}) + ivk}{(E - \varepsilon(\mathbf{k})) (E - \varepsilon(\mathbf{k} + \mathbf{Q}) + ivk) - |D|^2}. \quad (10)$$

Here $|D|$ stands for the amplitude of the fluctuating AFM order, $\varepsilon(\mathbf{k})$ is the electron energy in the paramagnetic phase,

$$v = |v_x(\mathbf{k} + \mathbf{Q})| + |v_y(\mathbf{k} + \mathbf{Q})|, \quad v_{x,y}(\mathbf{k}) = \frac{\partial \varepsilon(\mathbf{k})}{\partial k_{x,y}}. \quad (11)$$

In the absence of the damping the Green function (10) describes the electron in the spin-density wave state with the long-range order where Umklapp shadow band is given by $\varepsilon(\mathbf{k} + \mathbf{Q})$. On the other hand, for the AFM spin-liquid there is a dynamical transition $\varepsilon(\mathbf{k}) \rightarrow \varepsilon(\mathbf{k} + \mathbf{Q})$ with finite lifetime $1/\tau \sim vk$.

The paramagnetic dispersion is shown in Fig. 3a by a thin green curve and a shadow band by a dotted curve to stress that it has the finite lifetime as follows from equation (10). The resulting QP dispersion in the short-range AFM state is given by a thick blue curve. With increasing doping the Fermi level moves down from its initial value “0” in the Fig. 3a. The first intersection occurs along the $(0, 0) - (\pi, \pi)$ direction and results in 4 small hole pockets. The inner part of the FS is formed mainly by the non-damped electrons from the $\varepsilon(\mathbf{k})$ band while the outer part is formed mainly by the damped shadow band. That is why the outer part has a very small spectral weight and was not seen in ARPES data until recent discovery by the laser ARPES with the ultra-high energy resolution¹⁶ (see Fig. 1). This qualitative analysis reproduce the calculations^{12,13,14,15,46}.

Now we proceed to higher doping concentrations. For $x = 0.16$ where AFM correlation length $\xi_{AFM} \approx 10\text{\AA}$ we have two large FS centered around (π, π) . Those can be deduced from Fig. 3a by further decrease of the Fermi energy, μ . The critical point x_{c1} appears when μ touches the second peak along the $(\pi, \pi) - (\pi, 0)$ direction. It is clear from Fig. 3a that the inner FS will be of the electronic type and is formed by the damped shadow band. Thus the corresponding spectral peaks are very small. The outer FS is of the hole type and is formed by the non-damped states. That is why its intensity is much larger than that of the inner part (see Ref. 52 and Fig. 1 for $x = 0.16$). With further decrease of μ it will cross the bottom of the band at $x = x_{c2}$ and that corresponds to the collapse of the electronic FS. Finally at $x > x_{c2}$ the crossing of μ with the saddle point at $(\pi, 0)$ results in the transformation of the FS from the hole to the electron type at $x = x_{c3}$. Latter takes place in a strongly OD regime; this effect can be obtained in any conventional single electron approach and has been discussed before⁶⁹. For comparison, we present our calculated band structure for various doping concentration in Fig. 3b and the constant energy cut in Fig. 3c. It is clear that the rigid band approach of Fig. 3a may give the correct sequence of the FS reconstruction but quantitatively it is wrong.

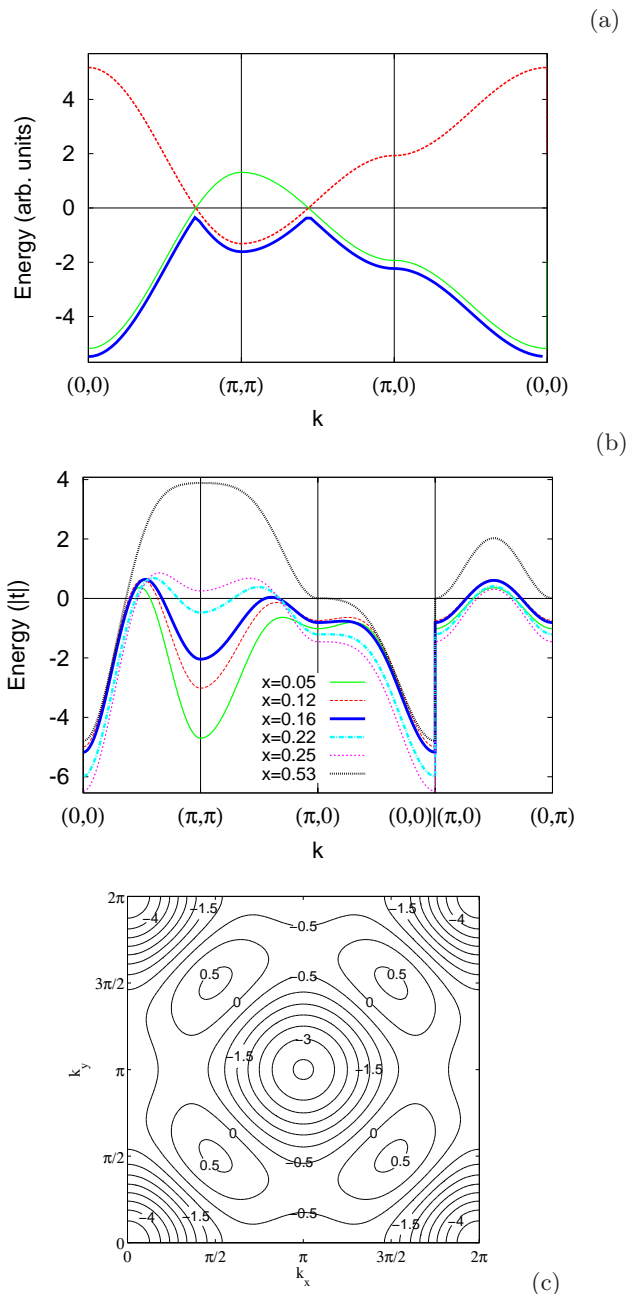


FIG. 3: A qualitative scheme of the band structure of the electron on the fluctuating AFM background (a), our calculations (b), and the constant-energy cuts for $x = 0.10$ (c). The zero energy in (b) and (c) corresponds to the Fermi level. The constant energy contours in (c) are labeled by the values of the corresponding energies (in units of t).

IV. LOW TEMPERATURE THERMODYNAMICS NEAR THE LIFSHITZ TRANSITION

According to Lifshitz results^{37,38}, both FS transformations at x_{c1} and x_{c2} are 2.5 order electronic phase transitions (nowadays the term QPT is used). Appearance of a new FS sheet at $\varepsilon = \varepsilon_c$ gives the additional den-

sity of state $\delta g(\varepsilon) = \alpha(\varepsilon - \varepsilon_c)^{1/2}$, with $\alpha \sim 1$ in a 3D system. In spite of a strong anisotropy in cuprates they are 3D crystals. Weak interlayer hopping results in a FS modulation along the k_z axis that has been measured by ARPES³³. That is why we can use results of Refs. 37,38 with minimal modification due to the QP spectral weight in the strongly correlated system $F_{\bar{\sigma}2} = (1+x)/2$.

Near the critical point the thermodynamical potential gains additional contribution:

$$\Omega(\mu, T) = \Omega_0(\mu, T) + \delta\Omega. \quad (12)$$

This singular contribution is induced by a new FS sheet at $\varepsilon > \varepsilon_c$ and is equal to

$$\delta\Omega = - \int_0^\infty \delta N(\varepsilon) f_F(\varepsilon) d\varepsilon, \quad (13)$$

where $f_F(\varepsilon)$ is the Fermi function. The number of states is given by

$$\delta N(\varepsilon) = \begin{cases} 0, \varepsilon < \varepsilon_c \\ \frac{2}{3}\alpha \frac{1+x}{2} (\varepsilon - \varepsilon_c)^{3/2}, \varepsilon > \varepsilon_c \end{cases} \quad (14)$$

At low temperature, $T \ll z$, $z = \mu - \varepsilon_c$, and close to the QPT at $z = 0$ we get

$$\delta\Omega = \begin{cases} -\frac{\sqrt{\pi}}{4}(1+x)\alpha T^{5/2} e^{-|z|/T}, z < 0 \\ -\frac{2}{15}(1+x)\alpha |z|^{5/2} - \frac{\pi^2}{12}(1+x)T^2 |z|^{1/2}, z > 0 \end{cases} \quad (15)$$

It is a $z^{5/2}$ singularity that tells about 2.5 phase transition. In our case z depends on doping so $z(x) = 0$ at $x = x_{c1}$ and $x = x_{c2}$.

The singular contribution to the Sommerfeld parameter $\gamma = C_e/T$ where C_e is the electronic specific heat, has the following form

$$\begin{aligned} \delta\gamma &= -\frac{\partial^2 \delta F}{\partial T^2} \\ &= \begin{cases} \frac{\sqrt{\pi}}{4}(1+x)\alpha \frac{|z|^2}{T^2} \left(1 + 3\frac{T}{|z|} + \frac{15}{4}\frac{T^2}{|z|^2}\right) e^{-|z|/T}, z < 0 \\ \frac{\pi^2}{6}(1+x)\alpha z^{1/2}, z > 0 \end{cases} \end{aligned} \quad (16)$$

We have deduced $z(x)$ dependence near each critical point from our band structure calculations. Obtained $\delta\gamma$ at $T = 10K$ near x_{c1} is shown in the Fig. 4. We also plot the experimental data³⁹ for LSCO, where C_e has been obtained by extrapolation of the high temperature data for $T > T_c$ to the low- T region. The experimental points in Fig. 4 correspond to the total γ ,

$$\gamma(x) = \gamma_0(x) + \delta\gamma, \quad (17)$$

where γ_0 is a smooth function at $x \approx x_{c1}$.

Since the electron FS pocket disappears for $x > x_{c2}$, for $x < x_{c2}$ our theory produce a singular behavior of $\gamma(x)$ corresponding to the case of $z > 0$. Measurements of the electronic specific heat⁵⁴ in NdBa₂Cu₃O_{6+y} revealed two weak maxima of $\gamma(x)$ at $p = 0.16$ and $p = 0.23$ that are close to our x_{c1} and x_{c2} . To stay away from the superconductivity, measurements of Ref. 54 were carried out at $T = 200K$ that explains why singularities appear as weak maxima.

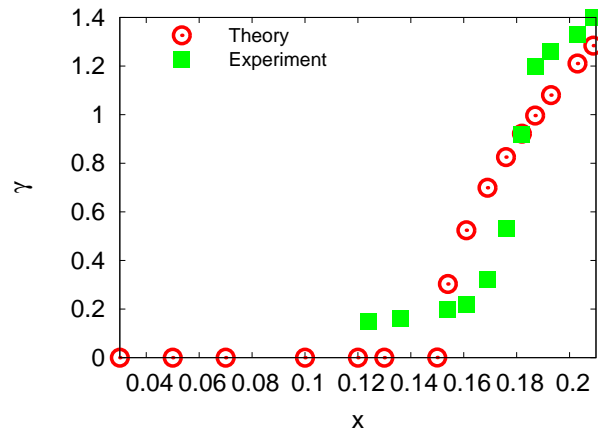


FIG. 4: The Sommerfeld parameter near the Lifshitz QPT. Experimental data for $\gamma = C_e/T$ at $T = 10K$ were taken from Ref. 39.

V. CONCLUSION

Previously, transformations of the FS has been discussed within a variational approach to the $t-J$ model²⁸. The small hole pocket near the $(\pi/2, \pi/2)$ point has been obtained in the UD AFM. At large doping, the electronic FS around $(0,0)$ point also has been obtained. Nevertheless, the FS for intermediate x in Ref. 28 does not correspond to our FS and to the experimental data.

Recently there were a lot of discussions on the change of the carrier sign upon doping. At large x , the FS becomes of the electronic type: in LSCO it happens at $x > 0.30$ ⁵⁵. As was mentioned above, it is rather a trivial fact. More unusual are the experimental data on the change of the Hall coefficient (R_H) sign in the UD systems. This effect was observed (under a strong magnetic field of $50 \div 60T$ that suppress the superconductivity) in YBa₂Cu₃O_y with $p = 0.10, 0.12$ and 0.14 ⁵⁶, and in LSCO with $p = 0.11$ ⁵⁷. All these crystals belong to the region $x < x_{c1}$ and according to our theory should have the small hole FS pockets. We believe that the arguments of Ref. 58 may explain the negative total Hall coefficient due to opposite partial contributions to R_H of the FS with opposite curvatures in the two-dimensional metal.

Low temperature transport measurements on La_{1.6-x}Nd_{0.4}Sr_xCuO₄ in a strong magnetic field up to 35T reveal the change of the FS topology at $p^* \approx 0.23$ ⁵⁹. This critical point is very close to our $x_{c2} = 0.24$. Also, our theory agrees with the data of Ref. 59 in the sense that at $p = 0.24$ the R_H indicates the large cylindrical FS with $1+p$ holes. At $p = 0.20$ that corresponds to $x < x_{c2}$, the $R_H(T)$ increase at low temperature leads to the conclusion that the FS reconstruction and pseudogap formation happen at $p < p^*$ ⁵⁹. The critical concentration x_{c2} agrees with the concentration $p_c = 0.23$ where the van Hove singularity in Bi2201 have been found in ARPES^{60,61}.

There is a wide discussion in the literature on the

quantum critical point P_{crit} where the pseudogap characteristic temperature $T^*(P) \rightarrow 0$. According to Ref. 62, $P_{crit} = 0.19$ and according to Ref. 63, $P_{crit} = 0.27$. All these values are obtained by extrapolation from finite- T regime. On the contrary, the two critical points x_{c1} and x_{c2} obtained here are the properties of the ground state and results from the Lifshitz QPT. It is well maybe that our x_{c2} is somehow related to the P_{crit} , at least $p^* = 0.24$ is related in Ref. 59 to the pseudogap formation at $p < p^*$.

Acknowledgments

We thanks A. Kordyuk for the discussion of results and T.M. Ovchinnikova for technical assistance. This work was supported by project 5.7 of the Presidium of RAS programm ‘‘Quantum physics of the condensed matter’’, RFFI grant 09-02-00127, and integration project N 40 of SB RAS.

-
- * Electronic address: shneyder@iph.krasn.ru
- ¹ E. Dagotto, Rev. Mod. Phys. **66**, 763 (1994)
 - ² E.G. Maksimov, Phys. Usp. **43** 965 (2000)
 - ³ M. Imada, A. Fujimori, Y. Tokura, Rev. Mod. Phys. **70**, 1039 (1998)
 - ⁴ S.G. Ovchinnikov, Phys. Usp. **40** 993 (1997)
 - ⁵ M.V. Sadvovskii, Phys. Usp. **44** 515 (2001)
 - ⁶ V.F. Elesin, V.V. Kapaev, Yu.V. Kopaev, Phys. Usp. **47** 949 (2004)
 - ⁷ Yu.A. Izyumov, E.Z. Kurmaev, Phys. Usp. **51** 23 (2008)
 - ⁸ P.A. Lee, Rep. Prog. Phys. **71**, 012501 (2008)
 - ⁹ A. Damascelli, Z. Hussein, Z.X. Shen, Rev. Mod. Phys. **75**, 473 (2003)
 - ¹⁰ N. Doiron-Leyraud et al, Nature **447**, 565 (2007)
 - ¹¹ E.A. Yelland, J.Singleton, C.H. Mielke, N. Narrison, F.F. Balakirev, B. Dabrowski, J.R. Cooper, Phys. Rev. Lett. **100**, 047003 (2008)
 - ¹² E.Z. Kuchinskii, I.A. Nekrasov, M.V. Sadvovskii, JETP Lett. **82**, 198 (2005)
 - ¹³ E.Z. Kuchinskii, M.V. Sadvovskii, JETP **103**, 415 (2006)
 - ¹⁴ N. Harrison, R.D. McDonald, J. Singleton, Phys. Rev. Lett. **99**, 206406 (2007)
 - ¹⁵ E.Z. Kuchinskii, M.V. Sadvovskii, JETP Lett. **88**, 192 (2008)
 - ¹⁶ J. Meng, G. Liu, W. Zhang et al., arXiv:0906.2682 (2009)
 - ¹⁷ M.Yu. Kagan, K.I. Kugel, Phys. Usp. **44** 553 (2001)
 - ¹⁸ S.G. Ovchinnikov, I.S. Sandalov, Physica C **161**, 607 (1989)
 - ¹⁹ S.V. Lovtsov, V.Yu. Yushankhai, Physica C **179**, 159 (1991)
 - ²⁰ J.H. Jefferson, H. Eskes, L.F. Feiner, Phys. Rev. B **45**, 7959 (1992)
 - ²¹ V.I. Belinicher, A.L. Chernyshev, V.A. Shubin, Phys. Rev. B **53**, 335 (1996)
 - ²² N.M. Plakida, V.S. Oudovenko, Phys. Rev. B **59**, 11949 (1999)
 - ²³ M.M. Korshunov, V.A. Gavrichkov, S.G. Ovchinnikov, I.A. Nekrasov, Z.V. Pchelkina, V.I. Anisimov, Phys. Rev. B **72**, 165104 (2005)
 - ²⁴ W. Stephan, P. Horsch, Phys. Rev. Lett. **66**, 2258 (1991)
 - ²⁵ R. Preuss, W. Hanke, W. von der Linden, Phys. Rev. Lett. **75**, 1344 (1995)
 - ²⁶ V.F. Elesin, V.A. Koshurnikov, J. Exp. Theor. Phys. **79**, 961. (1994)
 - ²⁷ B.I. Shraiman, E.D. Siggia, Phys. Rev. Lett. **61**, 467 (1988)
 - ²⁸ S.A. Trugman, Phys. Rev. Lett. **65**, 500 (1990)
 - ²⁹ A.F. Barabanov, Superconductivity: Physics, Chemistry and Technology **3**, 8 (1990) [in Russian]
 - ³⁰ A.F. Barabanov, R.O. Kuzian, L.A. Maksimov, J. Phys.: Condens. Matter. **39**, 129 (1991)
 - ³¹ A.P. Kampf, Phys. Rev. **249**, 219 (1994)
 - ³² G. Dorf, A. Muramatsu, W. Hanke, Phys. Rev. B **41**, 9264 (1990)
 - ³³ S. Sahrakorpi, R.S. Markiewicz, H. Lin et al, Phys. Rev. B **78**, 104513 (2008)
 - ³⁴ T.R. Thurston, R.J. Birgeneau, M.A. Kastner et al, Phys. Rev. B **40**, 4585 (1989)
 - ³⁵ S.M. Haden et al, Phys. Rev. Lett. **66**, 821 (1991)
 - ³⁶ D. Mihailovic, V.V. Kabanov, Superconductivity in Complex Systems. Series: Structure and Bonding, Vol. **114**, edited by K. A. Muller and A. Bussmann-Holder (Springer Verlag, Berlin, 2005), p. 331
 - ³⁷ I.M. Lifshitz, Sov. Phys. JETP **11** 1130 (1960)
 - ³⁸ I.M. Lifshitz, M.Ya. Asbel and M.I. Kaganov Electron Theory of Metals, Consultant Bureau, New York (1973)
 - ³⁹ J.W. Loram, J. Luo, J.R. Cooper, W.Y. Liang, J.L. Tallon, Phys. Chem. Solids **62**, 59 (2001)
 - ⁴⁰ Ya.B. Gaididei, V.M. Loktev. Phys. Stat. Sol. B **147**, 307 (1988)
 - ⁴¹ V.A. Gavrichkov, S.G. Ovchinnikov, .. Borisov, E.G. Goryachev, JETP **91** 369 (2000)
 - ⁴² J. Zaanen, G.A. Sawatzky, J.W. Allen, Phys. Rev. Lett. **55**, 418 (1985)
 - ⁴³ S.G. Ovchinnikov, V.V. Val’kov, Hubbard operators in the Theory of Strongly correlated electrons, Imperial College Press, London-Singapore, 2004.
 - ⁴⁴ R.O. Zaitsev, Sov. Phys. JETP **41**, 100 (1975)
 - ⁴⁵ M.M. Korshunov, S.G. Ovchinnikov, Eur. Phys. J. B **57**, 271 (2007)
 - ⁴⁶ N.M. Plakida, V.S. Oudovenko, JETP **104** 230 (2007)
 - ⁴⁷ V.V. Val’kov, D.M. Dzebisashvili, JETP **100** 608 (2005)
 - ⁴⁸ H. Shimahara, S. Takada, J. Phys. Soc. Jpn **60**, 2394 (1991); **61**, 989 (1992)
 - ⁴⁹ A.F. Barabanov, V.M. Berezovskii, JETP **79** 627 (1994)
 - ⁵⁰ A. Sherman. M. Schreiber, Phys. Rev. B **65**, 134520 (2002)
 - ⁵¹ A.A. Vladimirov, D. Ihle, N.M. Plakida, Theor. Math. Phys. **145**, 1576 (2005)
 - ⁵² M. Hashimoto, T. Yoshida, H. Yagi et al, Phys. Rev. B **77**, 094516 (2008)
 - ⁵³ M. Plate, J.D.F. Mottershead, I.S. Elfimov et al, Phys. Rev. Lett. **95**, 077001 (2005)
 - ⁵⁴ U. Tutsch, P. Schweiss, H. W?he, B. Obst, Th. Wolf, Eur. Phys. J. B **41**, 471 (2004)
 - ⁵⁵ I. Tsukada, S. Ono, Phys. Rev. B **74**, 134508 (2006)
 - ⁵⁶ D.Le Boeuf, N. Doiron-Leyraud, J. Levallois et al, Nature **450**, 533 (2003)
 - ⁵⁷ T. Adachi, T. Noji, Y. Koike, Phys. Rev. B **64**, 144524 (2001)

- ⁵⁸ N.P. Ong, Phys. Rev. B **43**, 193 (1991)
- ⁵⁹ R. Daou, N. Doiron-Leyrand, D. Le Boeuf et al, Nature Phys. **5**, **31** (2009)
- ⁶⁰ A. Kaminski, S. Rosenkranz, N.M. Fretweel et al, Phys. Rev. B **73**, 174511 (2006)
- ⁶¹ A.A. Kordyuk, S.V. Borisenko, M. Khupfer, J. Fink, Phys. Rev. B **67**, 064504 (2003)
- ⁶² J.G. Storey, J.L. Tallon, G.V.M. Williams, Phys. Rev. B **78**, 140506(R) (2008)
- ⁶³ S. Hufner, M.A. Hossain, A. Damascelly, G.A. Sawatzky, Rep. Prog. Phys. **71**, 062501 (2008)
- ⁶⁴ S. Sachdev, A.V. Chubukov, A. Sokol, Phys. Rev. B **51**, 14874 (1995)
- ⁶⁵ A.F. Barabanov, A.A. Kovalev, O.V. Urusaev, A.M. Belemuk, R. Hain, JETP **92** 677 (2001)
- ⁶⁶ L. Hozoi, M.S. Laad, P. Fulde, Phys.Rev.B **78**, 165107 (2008)
- ⁶⁷ M.M. Korshunov, S.G. Ovchinnikov, Phys. Sol. St. **45**, 1415 (2003)
- ⁶⁸ A. Ino, C. Kim, M. Nakamura *et al.*, Phys.Rev. B **65**, 094504 (2002)
- ⁶⁹ F. Onufrieva, P. Pfeuty, Phys.Rev.B **61**, 799 (2000)